4
Modelling Strength of Clay Ceramic Water Filtration Materials as a function of Surface Characteristics

4.1 INTRODUCTION

South Asia has a large rural population which predominantly lives at un-piped locations [Rosegrant and Binswanger, 1994]. Physical water scarcity superimposes on economic water scarcity at rural regions in South Asia [Plappally and Lienhard, 2013]. Different parts of India typically showcase such a scenario [Plappally *et al*., 2013]. Clay ceramics are accessible to this economically backward rural population [Saraswati, 1978]. Ceramics cover a wide range of applications due to their structural heterogeneity [Carty and Lednor, 1996]. Among the different class of ceramics, clay-based ceramics filters have proven to be sustainable solutions for drinking water [Sobsey *et al.,* 2008]. Several non-government organizations are spearheading dissemination of frustum-shaped clay ceramic water filter manufacture in several locations in India [Gupta *et al.,* 2016]. Scalability of these clay ceramic filters and use of different filter geometries is also sought for improving filtrate production with time [Murcott , 2006; Annan *et al*., 2016].

Traditionally potters provide importance to visual inspection of the fired material to judge its structural and functional quality. Therefore, this investigation is directed to study the relationship of the dimensional parameters such as porosity and surface roughness with material toughness, load-bearing capacity, and functionality.

Ceramic water filter manufacture requires native clay and plant-based waste residues as input raw materials. The residues of agriculture and carpentry waste have been incorporated as raw materials [Prasad and Ganvir, 2006]. The properties of clay and filler residues differ with geographical location [Lark and Webster, 2001; Higashikawa *et al*., 2010]. The strength of ceramics is influenced by the chemical composition and porous fraction [Cultrone *et al*., 2004; Lange, 1989]. Relating the strength of ceramics to its surface properties and microstructure is very important for functional applications [Tay, 1987; Lohbauer *et al*., 2008]. Modification of the material surfaces relates to changes in surface energy which affects properties of wettability and adhesion [Lawrence and Spencer ,1999; Shuttleworth and Bailey, 1999]. Furthermore, materials have distinct hydrophobic and hydrophilic properties depending on different surface roughness and capillary pore contact angles [Gajewski, 2008]. Bio-receptivity and microbial adhesion can be improved by increasing surface roughness in porous ceramics like roof tiles [Gazulla, 2011]. Therefore, pore features and surface roughness of materials have some correlations.

The porosities are direction dependent parameters [Narasimhan , 2013]. Liu [Liu, 1997] provided a polynomial expression of compressive strength as a function of porosity in hydroxyapatite based ceramics. The increase of porosity leads to a decrease in resistance to crack propagation in clay ceramics used for filtering water [Yakub and Soboyejo, 2013]. It is known that pore geometry such as pore orientation angle can be used to predict Young's modulus [Boccaccini, 1998]. The fracture toughness was also expressed as a power law of the pore sizes found within the clay ceramic [Maiti *et al*., 1984; Sin *et al*., 2012; D'Orazio *et al*., 2014]. Fracture toughness was found to be better predicted using pore dimensions than porosity [Plappally *et al*., 2018]. Recently, Plappally et al. [Plappally *et al*., 2018] provided a multi-parameter stochastic formulation for fracture toughness as a function of the composition of the raw material used to manufacture the clay ceramic.

The different sections below will enumerate laboratory studies on the chemical characteristics of square plate water filtration clay ceramics. Compositional correlations which affect sintering and mechanical properties were investigated [Kramer, 1985]. The effect of

porosity and surface roughness of these clay ceramics due to raw material composition was substantiated. The structural quality of the filter using simple visual surface profiling was carried out and elaborated. Discharge through square plate water filters containing 20cm of water is modelled and compared with cylindrical and frustum shaped filters with a water column height of 20cm [Gupta *et al.*, 2016]. The results of the studies imply providing notion towards possible scaling of such ceramic devices [Annan *et al.*, 2016; Kaurwar *et al.*, 2017]

4.2 MATERIAL AND METHODS

4.2.1 Clay and its characteristics

The clay samples were obtained from a clay mining area in Mokalsar, Jodhpur, Rajasthan. The local clay samples obtained are coarse in size. These samples are powdered manually using a wooden mallet and controlled in size using 35 meshsize. The fluorescence spectroscopy based investigation of chemical constituents (Bruker S4 Pioneer facility X-ray fluorescence) of clay is given in **Table 4-1**. It is observed that silicates, aluminates, oxides of iron, and salts dominate the clay composition. Due to direct extraction, a large quantity of organics is also found within the local clays. Magnesium oxide content in the local clays is more than in Illite and lower than in montmorillonite and metabentonite. Sodium oxide content is closer to that in Illite and lower than montmorillonite [Carroll and Starkey, 1971].

Table 4-1 : Chemical composition of clay

Chemical Compounds	Loss on Ignition	SiO_2	Al_2O_3	Fe_2O_3	CaO	K_2O	MgO	Na_2O	P_2O_5	TiO_2
Weight (%)	31.026	43.57	11.45	5.800	2.840	2.02	1.710	0.530	0.060	0.650

4.2.2 Sawdust as organic filler

The saw dust used in this work was obtained from Rajasthan Timber, Jalori Gate, Jodhpur. This sawdust is 90% acacia wood (imported from Ghana). The sawdust is brought and sieved using 18 mesh size sieve.The X-ray fluorescence spectroscopy investigation of sawdust is given in **Table 4-2**.

Table 4-2 : Chemical composition of organic filler

Chemical Compounds	Loss on Ignition	SiO_2	Al_2O_3	CaO	Fe_2O_3	K_2O	MgO	P_2O_5	TiO_2
Weight (%)	91.938	5.77	0.160	0.990	0.680	0.240	0.050	0.030	0.040

4.3 PREPARATION OF POROUS CLAY CERAMICS

Mixtures containing local clay (C) and sawdust (O) in the volumetric ratio of (C:O) 65:35, 55:45, 50:50, 45:55, and 35:65 were prepared [Plappally *et al.*, 2010] (**Figure 4-2**). Precisely, 800 ml, 840 ml, 850 ml, 880 ml, and 890 ml of water was added in 1,600 ml volume of each of the respective mixtures before mixing.The mixing was performed manually using hands to attain homogeneity in the composition of the individual dough balls [Plappally *et al.*, 2010].

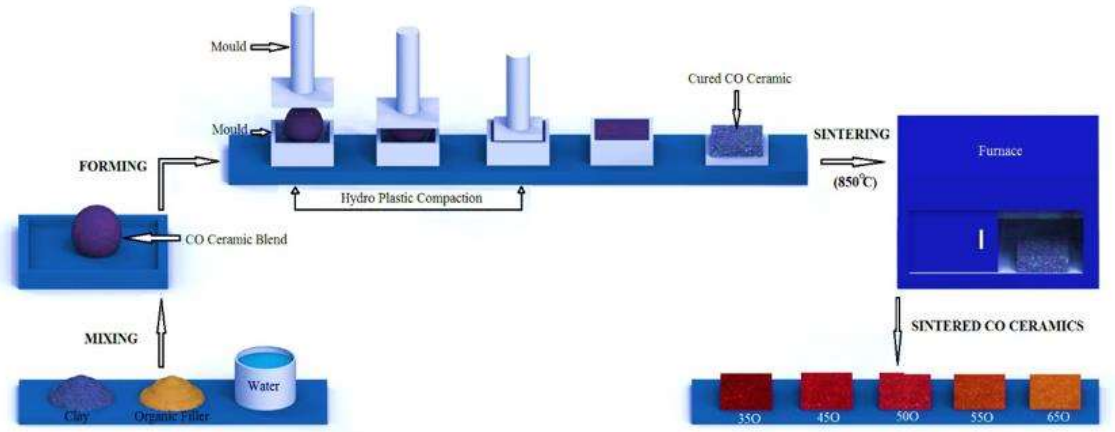

Figure 4-1 : Manufacturing of clay ceramics with distinct organic fraction

The moist dough was pressed under 1.5 bar pressure to form the green composites. The dimensions of the prepared green composites samples were 15 mm in thickness and 100 mm × 100 mm in cross-section. Furthermore, the samples were left for curing at room temperature until their weights stabilized. The dried samples were sintered in a programmable electric furnace [TEXCARETM Muffle Furnace 220V, 250×340×180 mm^3 (w×d×h)] at a temperature of 850°C [Plappally *et al*., 2018]. The weights of the dried and sintered green composites are shown in **Figure 4-2**, where the notations of 35O, 45O, 50O, 55O, and 65O represent the composites manufactured from the 65:35, 55:45, 50:50, 45:55, and 35:65 mixtures, respectively. The percentage weight reduction of the sintered samples with respect to dried samples were 20.1%, 30.6%, 41.6%, 42.1% and 49.3% for the 35O, 45O, 50O, 55O and 65O mixtures, respectively. The investigation into the correlations between microstructural and surface properties of the sintered samples were performed and is presented in the following sections.

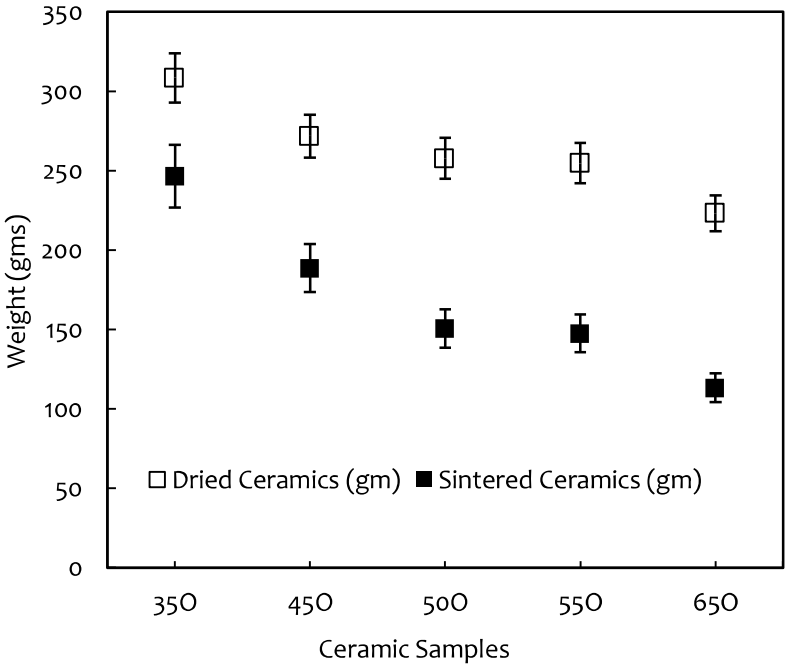

Figure 4-2 : Weight variation before and after sintering

4.4 CERAMICS CHARACTERIZATION

4.4.1 X-ray fluorescence

The different sintered CO ceramic samples were individually powdered using agate mortar and pestle. Powdered sample (2 mg) was mixed with 20 mg of boric acid and the mixture is turned into a pellet using pellet presser. The pellets were analyzed in Bruker S4 Pioneer X-ray fluorescence instrument at the Jawaharlal Nehru University, Delhi, India for determining the chemical composition of samples.

4.4.2 X-ray diffraction

The mineralogical investigation of ceramic samples was carried out in Bruker D8 advanced diffractometer using Cu-Kα radiation (λ = 1.5418) with a step size of 0.02 and scan speed of 0.5. Quantification of different minerals from the diffraction data was carried out using crystallographic analysis software (PANalytical X'pert High Score, PANalytical) [Degen *et al*., 2014].

4.4.3 Micro-structural characterization

The microstructural and densification behavior of CO ceramics were assessed using a scanning electron microscope. The ceramics were cut into 5 mm × 5 mm cross-section. Specimens were coated with palladium by low vacuum sputter coating in order to increase the conductivity of the sample to obtain superior image quality. The palladium coated CO ceramics were placed over the specimen slots which were covered with carbon tape and locked in the chamber for imaging analysis [Lyman *et al.,* 2012].

4.4.4 Physical property investigation

Porosity

The porosity and poresize distribution in distinct CO ceramics were determined using the Mercury Intrusion Porosimetry (MIP), Micromeritics AutoPore IV 9500 Series, I.I.T. Bombay, India. The MIP measurements were conducted on ceramic pieces with dimensions of 3 mm × 3 mm cross-section and were replicated three times for each sample. A sample set of 3 mm× 3 mm cross section was tested for mean orientation of pores using synchrotron-based micro-computed tomography technique (BL-4 Indus 2, RRCAT Indore, India operating at 2.5 GeV, 200 mA). The micro-CT image data sets were binarized to segment the pores using a sequence of distance transformation followed by watershed segmentation method [Schladitz, 2011]. The segmented pores were uniquely labelled to determine their frequency distribution over clay matrix surface. All operations of image processing and image analysis were carried out using open source software ImageJ [Rasband, 2011]. Apart from the measurement of pore dimensions the results were used to calculate permeability [Gupta *et al.*, 2016].

Surface Roughness

Samples of 50 mm × 50 mm cross section were kept under non-contacting optical profilometer (Bruker GT-KO, IIT Kanpur) to analyze the surface roughness profile of the different ceramic samples. The surface roughness is evaluated at 30 distinct points over the cross-section. The surface roughness measurements conformed to the methods for measuring surface texture (IS-25178-604 ISO international standard).

4.5 MECHANICAL CHARACTERIZATION

4.5.1 Fracture toughness test

The fracture toughness tests were carried out on laboratory-based universal testing machine (Model EZ-50, Lloyd instruments, Germany). The single edge notch bend (SENB) specimens were of 75 mm × 15 mm × 15 mm in size. The specimens showcased a notch width of 4 mm and a depth of 0.75 mm at the centre. A loading rate of 0.1 N/s was applied during the three-point bend tests [Plappally *et al*., 2010]. The test results corresponding to the fracture (ASTME-399-90 mode I test standard) were recorded using Nexygen material testing software (Nexygen plus 01/3366, Lloyd Instruments, Germany).

4.5.2 Compression Test

For the compressive strength test, ceramic specimens of 35 mm × 15 mm × 15 mm size were cut and extracted (Bosch GDC 120). A loading rate of 0.1 N/s was applied along the 35 mm axis until the sample was completely crushed. Load and strength data was recorded digitally using Nexygen plus material testing software. The compression tests conformed to ASTM 1358.

4.6 RESULTS AND DISCUSSION

4.7 FLOW MODELING

Hydrodynamic models are used to predict the flow of water through the filters with shapes as illustrated in **Figure 4-3** [Yakub and Soboyejo, 2012;Van, 2006; Carlson *et al*., 2008]. Different shapes are assumed to compare the volumetric variation in discharge. Filtration is assumed to follow Darcy's flow. Filtrate production of 650ml/hr to 965ml/hr from the use of local frustum shaped ceramic filter had been observed [Gupta *et al*., 2016]. The porous ceramic media permeability k of 8.1E-14 m² has been utilized to model the flow [Gupta *et al*., 2016]. The total flow through the geometries in **Figure 4-3** can be written as

$$Q_{total} = Q_{base} + Q_{side} \tag{4.1}$$

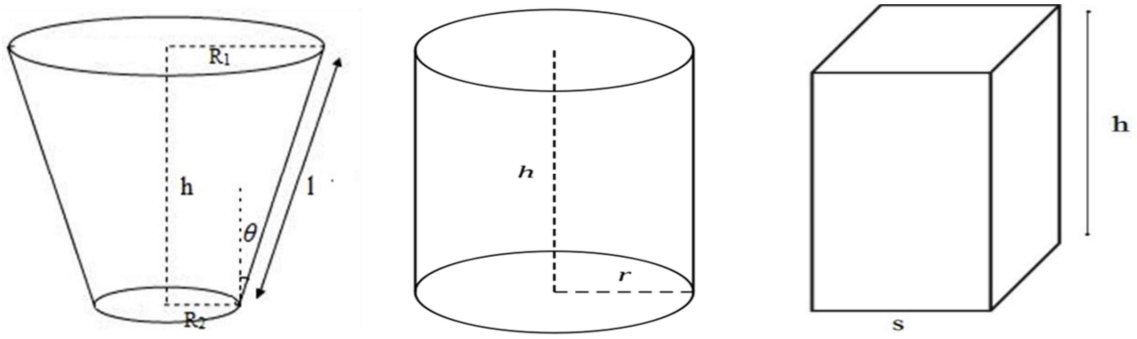

Figure 4-3 : The schematics of the assumed volumes of a frustum, cylinder and square base prism

For a frustum of height h, slant height l and a top and base radius for R1 and R2 respectively the total discharge Q_{total} will be a sum of Eq. (4.2) and Eq. (4.3).

$$Q_{base} \quad \frac{k}{\mu t_b}\pi {R_2}^2 \rho g h \tag{4.2}$$

$$Q_{side} \quad \frac{k}{\mu t_s}\int_0^h \rho g(h-z)\times 2\pi(R_1 + z\tan\theta)\frac{dz}{\cos\theta}$$

$$\frac{\pi k\rho g h l}{3\mu t_s}[2R_2 + R_1] \tag{4.3}$$

Here k is the permeability of the material, μ is the dynamic viscosity of the water is 8.935e-4 Pa.s at 25°C, t_b and t_s is the thickness of the base and the sides of the geometry respectively.

For a cylinder of height h and a radius for r the total discharge Q_{total} will be a sum of Eq. (4.4) and Eq. (4.5).

$$Q_{base} \quad \frac{k}{\mu t_b}\pi r^2 \rho g h \tag{4.4}$$

$$Q_{side} \quad \frac{k}{\mu t_s}\int_0^h \rho g(h-z)\times 2\pi r dz = \frac{\pi r k\rho g h^2}{\mu t_s} \tag{4.5}$$

For a square base prism of height h and a base side s respectively the total discharge Q_{total} will be a sum of Eq. (4.6) and Eq. (4.7).

$$Q_{base} \quad \frac{k}{\mu t_b}s^2 \rho g h \tag{4.6}$$

$$Q_{side} \quad \frac{k}{\mu t_s}\int_0^h \rho g(h-z)\times 4s dz = \frac{2sk\rho g h^2}{\mu t_s} \tag{4.7}$$

Darcy flow extensions from Eq. (4.2) to Eq. (4.7) have been used to retrodict the flow through ceramic filter geometries at 25°C [Gupta *et al.*, 2018].

4.7.1 X-ray fluorescence

The chemical composition of ceramics prepared from different compositional ratios is shown in **Figure 4-4** below. The sintered ceramics predominantly contained SiO_2, Al_2O_3 and Fe_2O_3. The percentage of silica, alumina, and oxides of iron decreased with increase in organic fraction in the fired (dried) ceramics. The presence of relatively high amount of silica, alumina, and quartz in the 35O, 45O and 50O samples, compared to the 55O and 65O samples (Fig. 3), will contribute to the physical properties of ceramics [Milheiro *et al.*, 2005]

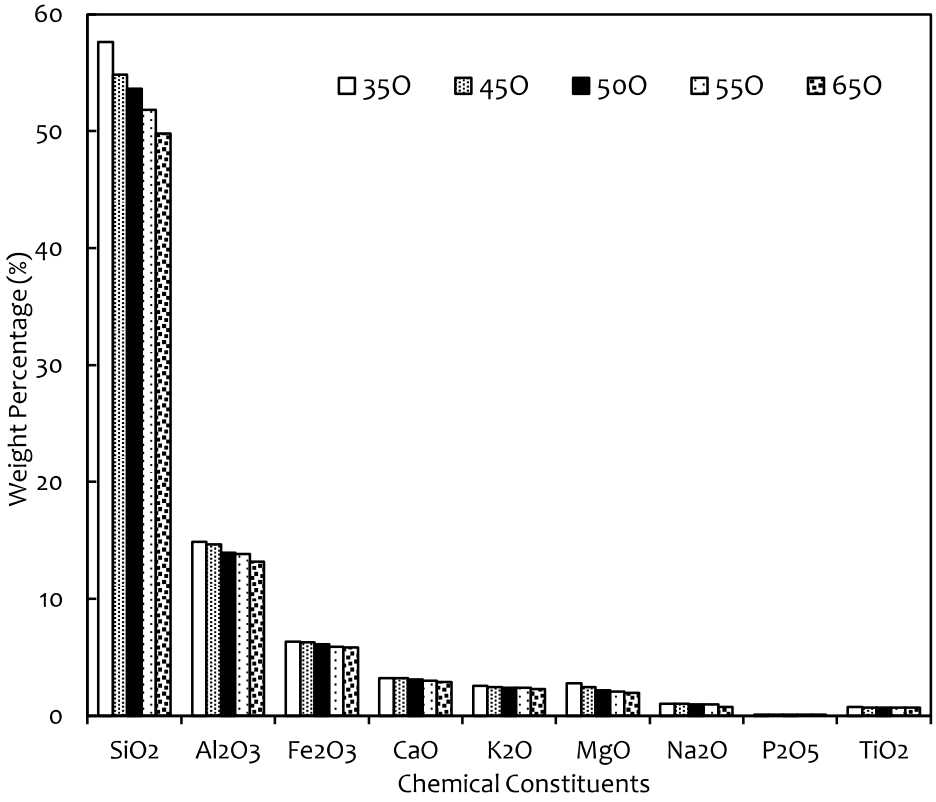

Figure 4-4 : Chemical composition of the Porous Clay Ceramics

The chemical composition data for clay was appended with that for the five porous clay ceramics and plotted in **Figure 4-5**. There are 9 variable chemical constituents or minerals (listed along the abscissa of the plot in **Figure 4-5**) in each of these six major materials. This provides the 6×9 compositional data matrix for the six major materials considered here. A multivariate analysis of the compositional data was performed (Minitab Version 16, Minitab Inc.). These chemical compositions were correlated to each other, which should be manipulated to utilize these variables in the prediction of any of the major properties of these ceramics [Soboyejo *et al.,* 2001; Haan, 1994].

A new uncorrelated matrix is derived from the correlated matrix of compositional data of clay (1), 35O (2), 45O (3), 50O (4), 55O (5) and 65O (6) using principal component analysis [Haan CT, 1994]. The analysis treats the correlation matrix using a characteristic value Eq. to find the independent matrix of variables and eigenvalues [Soboyejo *et al.,* 2001]. The new independent matrix elements correspond to the principal components which express the correlation magnitude [Plappally *et al.*, 2011;Soboyejo *et al.*, 2001]. The eigenvalues are 5.99936, 0.00050, 0.00010, 0.00003, 0.00001 and 0.00000 [Minitab v16]. The first component and second component are found to have corresponding high scaling factors or eigenvalues [Guigue *et al.*, 2013]. Therefore these two components were used to explain the effects of the chemicals on each other [Pullanagari et al., 2012].

The sign of each element defines the manner in which each of the chemical components contributes to its independent influences on the ceramic material characteristics [Plappally *et al*., 2011]. **Figure 4-5** illustrates positivity in the second component due to the presence of Na_2O and K_2O. Furthermore, the negativity of the second component is due to high Fe_2O_3, which is also the reason for the red color of the samples [Haan, 1994]. The CaO and MgO values also influence this negativity and indicate presence of traces of carbonates such as calcites [Pullanagari *et al*., 2012]. The small angles between Na_2O-K_2O, and CaO-MgO compositions signify the high correlation influencing microstructural properties of these local clay ceramics [Guigue *et al*., 2013]. This also confirms a similarity in their mode of influence [Papachristodoulou C *et al*., 2006]. Therefore, Na_2O-K_2O and CaO-MgO is said to be a prominent group or cluster which defines the presence of salinity in clays and influence its related ceramic properties.

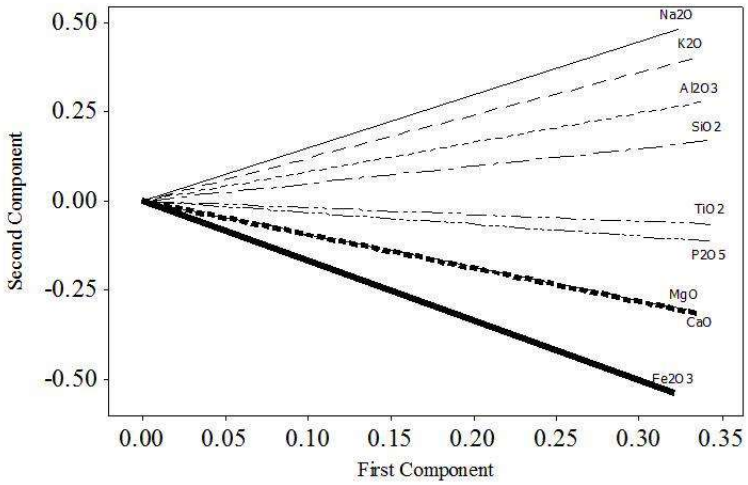

Figure 4-5 : Loading plot showing the Influence of chemicals on the micro-structural properties of clay ceramics [Minitab 16]

The derived two principal orthogonal components define a plane of nine different chemical compositions. The coordinates of all the chemical compositions on this plane are projected values known as scores [Eriksson *et al*., 2006].The score plot in **Figure 4-6** confirms clear distinction of properties between clusters 2-3 and 5-6. The ceramics with compositions of 2 and 3 would showcase similar properties. The 50O (4) composition has a very distinct structural character compared to these clusters [Pullanagari *et al*., 2012]. This hypothesis will be reflected in further micro-structural investigation. The properties of the six samples clearly lie disconnected from each other. Here, the properties of 1 (clay) and 4 (50O) can be said to be inversely correlated since they are located at quadrants which are diagonally opposite to each other [Eriksson *et al*., 2006].

This would mean that some properties of 4 will not change even if its composition has drastically changed from 1. Further, the closeness of 4 (50O) to the origin of score plot also suggest possible mirroring of sintered clay character [Satankar *et al*., 2017].

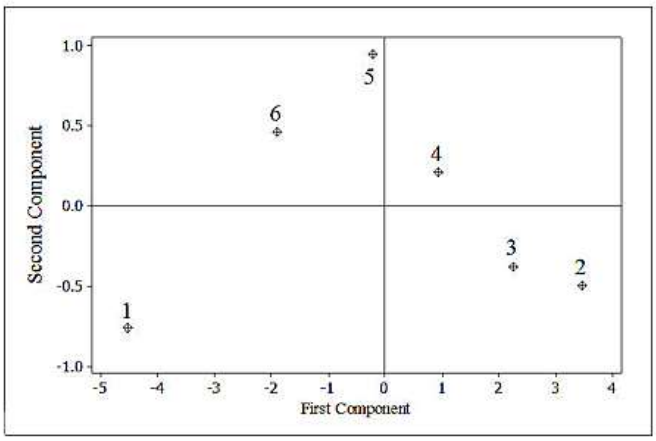

Figure 4-6 : The score plot of the principal components of the correlated matrix of elemental compositions of: Clay (1), 35O (2), 45O (3), 50O (4), 55O (5) and 65O (6), respectively [Minitab 16]

4.7.2 X-ray diffraction

The evolution of quartz, potassium feldspar, and hematite as prominent minerals within sintered ceramics can be observed from **Figure 4-7** [Manoharan *et al*., 2012]. The presence of high amount of silica is indicative of the occurrence of the quartz phase in ceramics. The presence of quartz influences the mechanical properties of fired ceramics [Schultz, 1964]. The appearance of feldspar aided densification and reduced sintering time [Kilikoglou *et al*., 1998; Wu *et al*., 2014; Kaurwar *et al*., 2017].

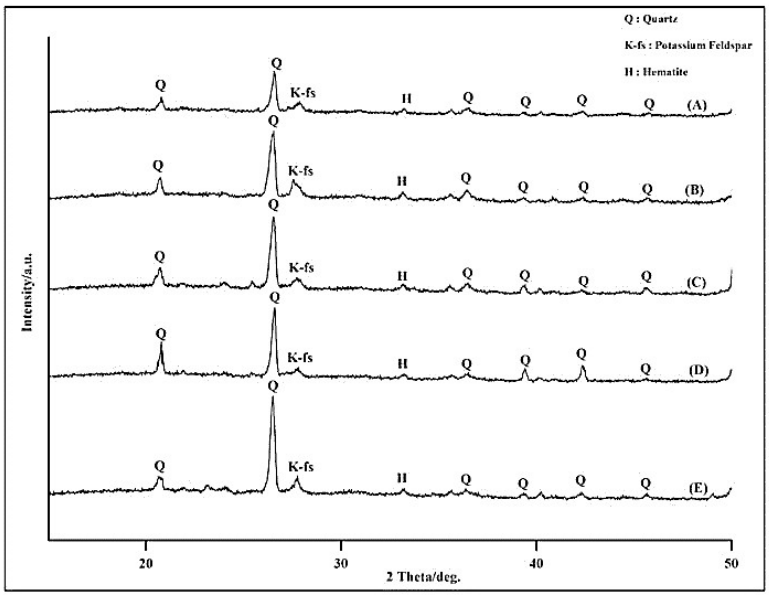

Figure 4-7 : X-ray diffraction pattern of fired ceramics prepared from different raw material compositional ratios (A) 65 O, (B) 55O, (C) 50O, (D) 45O, and (E) 35O [Origin Pro 16, IIT Jodhpur License]

The significant changes in the intensities of quartz peaks attribute to the varying clay-organic additive ratios. Clay ceramic water filter introduced in Rajasthan following the 50O composition developed cracks due to thermal stress [Gupta *et al*., 2018]. The fact being that clay artefacts do not show resistance to thermally induced stresses and hence a calcium carbonate addition was prescribed in this region to restrict high expansion rates of quartz [Buys and Oakley, 2014; Kaurwar *et al*., 2018]

4.7.3 Micro-structural analysis

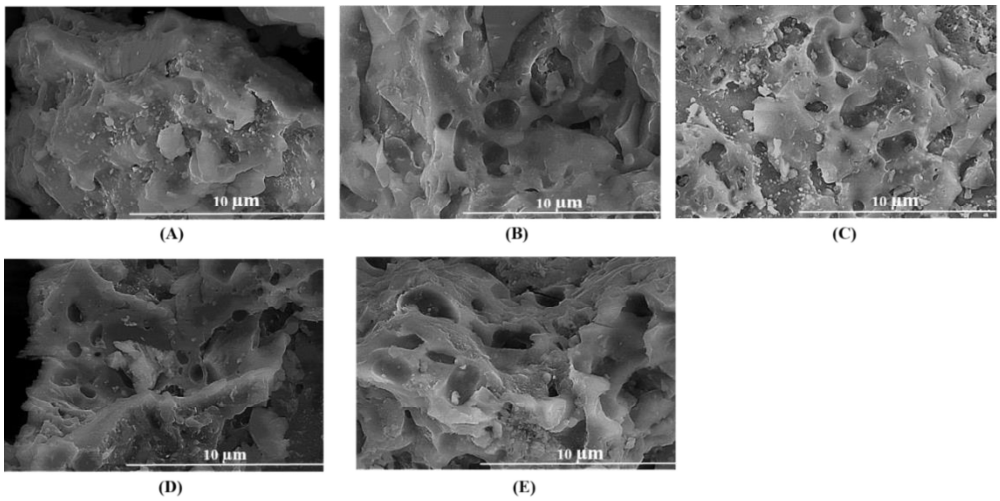

Figure 4-8 : Surface Morphology of distinct Porous clay ceramics at 5000X: A) 35O, B) 45O, C) 50 O, D) 55O, E) 65 O

The microstructure displays the presence of the pores and interconnected tunnels through the pores. The percentage of organic filler in the ceramics plays a crucial role in the porosity and the microstructure gets more open with high organic content (**Figure 4-8** and **Figure 4-9**) [Obada *et al.*, 2017].

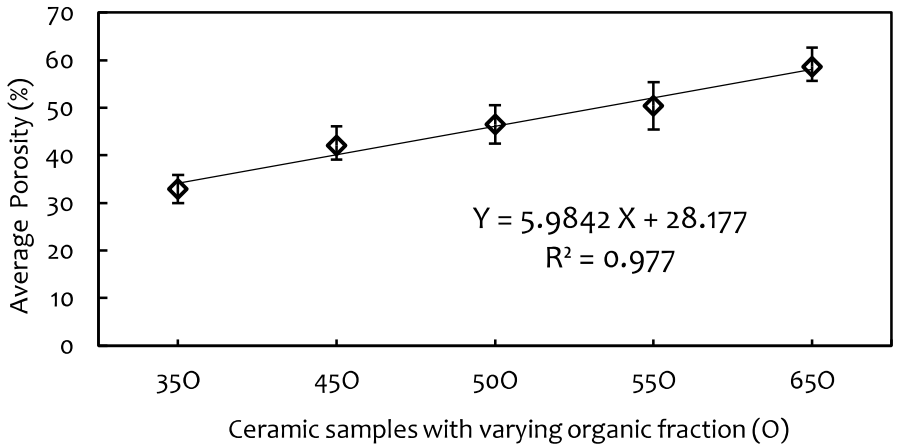

Figure 4-9 : Porosity variation with different ceramic composition

A linear relationship between the porosity and the composition of the clay ceramics is observed in **Figure 4-9**. [Plappally *et al.*, 2011]. The samples investigated were having pore sizes ranging between 0.003 – 360 µm.

Figure 4-10 presents the large porosity contribution due to the existence of submicron range pores and pore sizes between 1-5µm for 50O ceramics in comparison with other ceramic compositions. This would help to efficiently filter submicron size particles [Youmoue *et al.*, 2017].

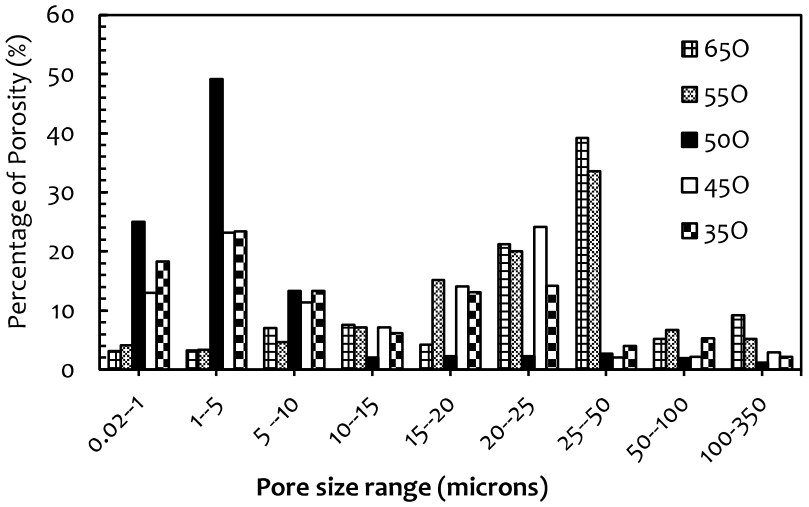

Figure 4-10 : Pore-size distribution for ceramics with distinct organic filler (O) content

The distribution of the orientation angle shown in **Figure 4-11**, confirms the randomness of the pores irrespective of their compositions. The area under the curves shows that there is a high density of pores orthogonal to the surface [Robertson *et al.*, 2015]. Pores perpendicular to filtration surfaces can be the best location for reactions and would positively influence the filtration and percolation. The area under the orientation angle curves corresponding to angles between 85°-105° is the maximum for 50O ceramics compared to the other ceramics analyzed through the information in Fig. 10. This characterizes the family of CO ceramics to be good for separating the solutes from the solutions and 50O is an efficient filtration material [Wooten, 2014]. Furthermore, it is to be noted that, if the pore orientation angles are as high as 90°, the physical properties of the porous material is enhanced with increasing aspect ratio [Griffiths *et al.*, 2017]. The frequency, at which these angles are detected within a specific clay ceramic sample, will influence their overall strength parameters [Griffiths *et al.*, 2017]. Therefore, the pore orientation angle data has to be utilized effectively to predict individual porous material properties.

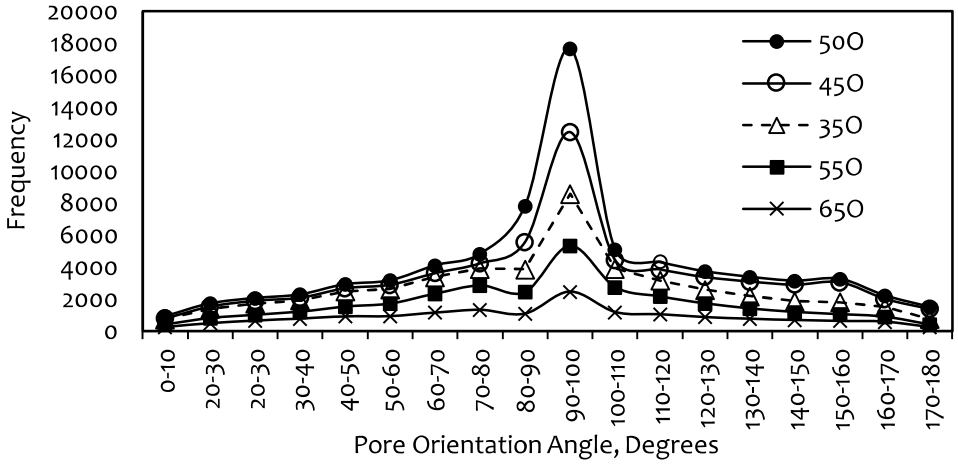

Figure 4-11 : Pore orientation in porous ceramics with distinct organic filler content

4.7.4 Surface roughness

The plot of the surface roughness of the different ceramics as a function of their corresponding porosities shown in **Figure 4-12** appears to be a straight line. The constant term in the Eq. indicated the role of intrinsic clay pores whose appearance is independent of the presence of the organic filler in developing the surface roughness in CO ceramics [Servi, 2013].

The surface flaws can influence the strength of ceramic material [Teughels *et al*., 2006]. Surface roughness degrades mechanical properties of a material product [Tay, 1987]. The porosity can be a function of the material microstructure, its manufacturing process, and material property [Shao *et al*., 2015; Jones and Ashby, 2005].

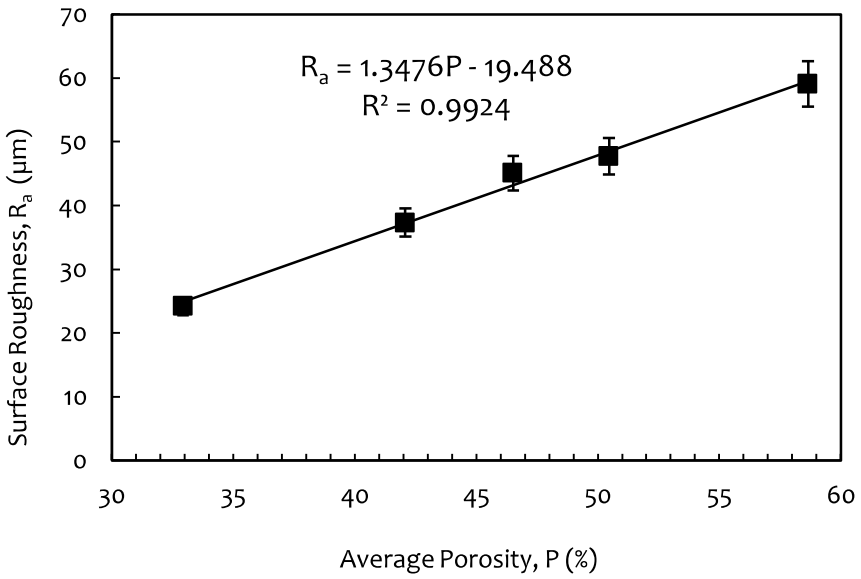

Figure 4-12 : Surface roughness variation with average porosity

4.7.5 Compressive Strength

The compressive strength displayed polynomial decrement with increasing organic filler fraction in the clay matrix (**Figure 4-13**). This linear decrement is supported by the fact that increasing the apparent porosity may result in decreasing the load bearing capacity [Kaurwar *et al.,* 2017]. The cracks present in the CO ceramics extended slowly and might propagate along the compressive axis to form the crushed zone, which promoted the compressive failure [Jones and Ashby, 2005;Davidge and Evans, 1970]. The degree of crack resistance or propagation is associated with the occurrence of the flaws and their pore size, meaning there is a possibility that compressive strength is related with the fracture toughness [Soboyejo, 2002]. This would mean that for the assessment of K_{IC}, we should concentrate on flaw size and their orientation which are basically pore size and their orientation angles [Liu, 1997; Jones and Ashby, 2005].

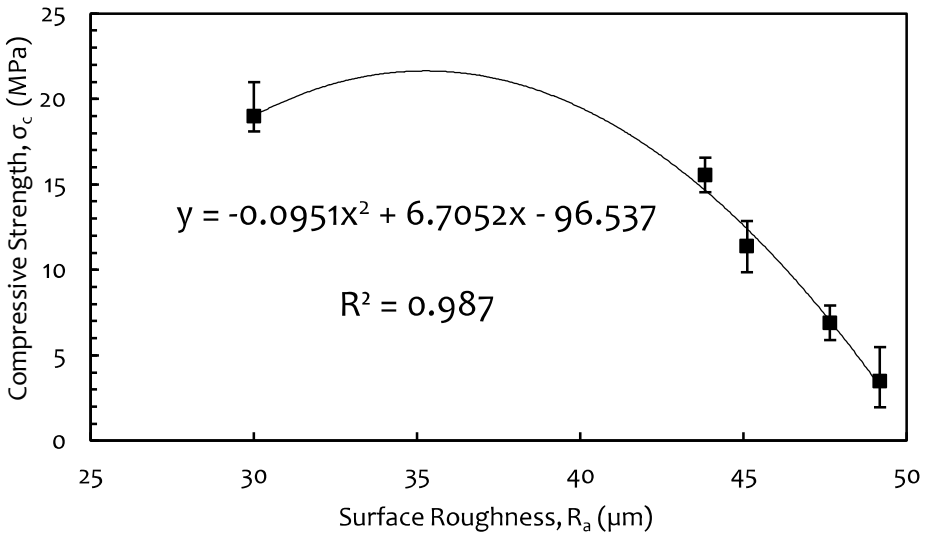

Figure 4-13 : Compressive strength as a function of surface roughness

The magnitude of compressive strength of different porous clay ceramics was found to be almost twice in comparison with the values of various clay-based water filters manufactured in different locations [Yakub, 2012; Plappally, 2010; Annan *et al.,* 2014]. This emphasises the geographical significance of the raw materials, process variables adopted, and thermal cycle temperature for the manufacturing of clay-based ceramics.

4.7.6 Fracture toughness

The average fracture toughness K_{IC} is plotted against surface roughness in **Figure 4-14**, which is fitted with the linear function. This approves the fact that a potter can visually interpret the toughness of the ceramic product. The model in **Figure 4-14** has the coefficient of determination of 0.9416. Earlier, the fracture toughness of fired clay ceramics was found to vary exponentially with sintering temperature [Sin *et al.,* 2012; Lee and Yeh, 2008; Freiman, 1981]. Also, the toughness of ceramics was found to influence by quartz content. Improvement in quartz content ensured the toughening of the material during fracture [Buys and Oakley, 2014].

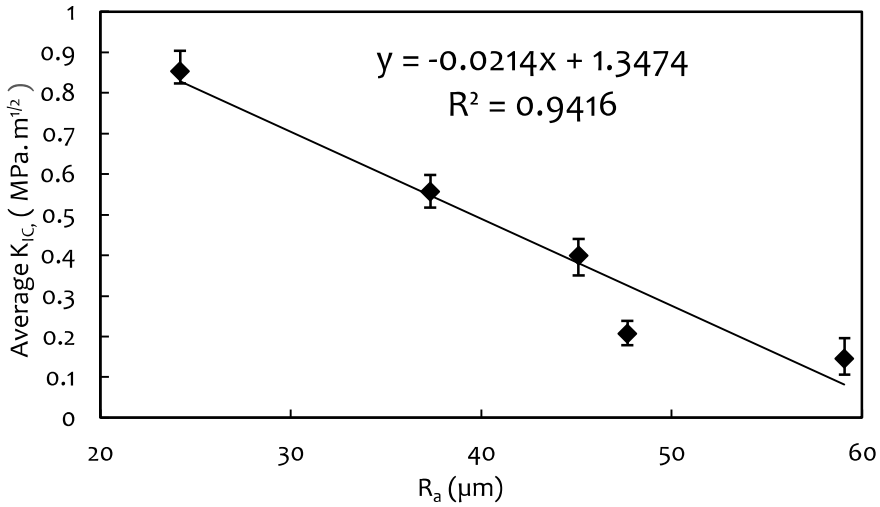

Figure 4-14 : Fracture toughness as a function of the surface roughness.

4.7.7 Prediction of K_{IC} on the basis of raw material quantity

Furthermore, the property of toughness of clay ceramics was said to be a power law function of porosity for a specific clay ceramic tile [Maiti *et al.*, 1984]. However, the fracture toughness Y is found to be predicted effectively using only the volume fraction of the organic material or sawdust X_1 than the porosity.

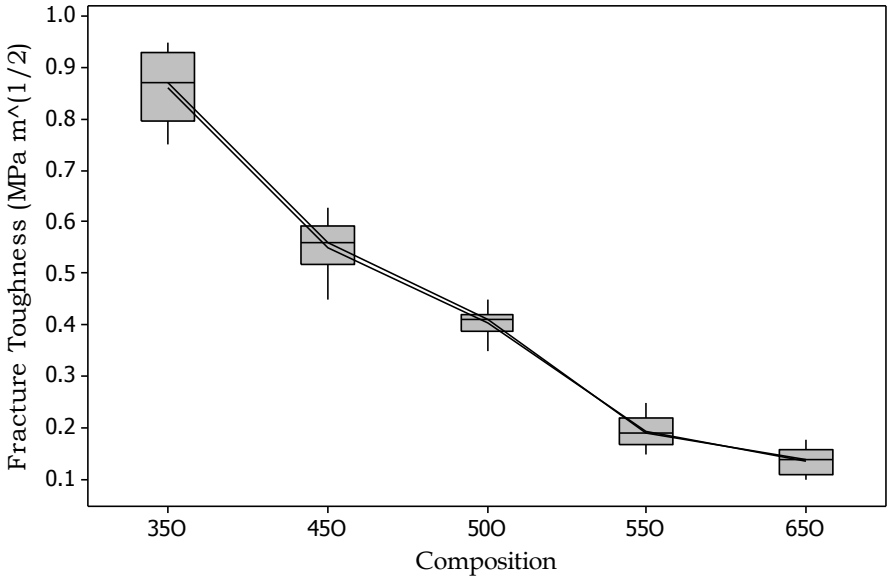

Figure 4-15 : Fracture toughness as a function of the percentage of organic fraction (sawdust)

The volume fraction of the sawdust X_1as a predictor of K_{IC} (Y) is expressed using a linear transformation [Natrella, 1963]

$$Y = a + c\left(X_1^b\right) \tag{4.8}$$

Table 4-3 : Modelling of the fracture toughness (Y) using Eq. (H).

Samples	$Y = a + c(X_1^b)$	R^2	Error, S	D_n	$D_n^{\alpha=99\%}$	KS test
All	$Y = 5.25 - (X_1^{1.24})$	93.8	0.066	0.14619	0.1718	Acceptable

Table **4-3** illustrates that linear transformation in Eq. (4.8) is found acceptable from the Kolmogorov-Smirnov test on fracture toughness data for ceramics produced. Therefore the assumed distribution of fracture toughness in Eq.(4.8) is accepted at a confidence interval level of 99% [Ang and Tang, 1975].

4.7.8 Flow Analysis

Flow from the clay ceramic filter geometries of frustum, cylindrical and square prism shape is represented in Fig. 14. Darcy flow Eq. is derived according to distinct geometries prism,

frustum and cylinder and stated in Eq. 4.2 to Eq. 4. 7 have been used to illustrate the flow through ceramic filter geometries at 25°C [Gupta *et al.*, 2018]. The square base prism provides a comparatively better discharge as compared to other geometries. It is important to note that a variation in shape may influence the discharge from the filters. An opportunity of scaling such filter is observed with varying filtrate discharge with dimensional changes.

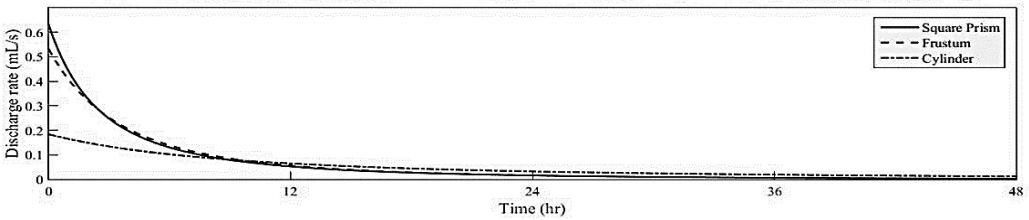

Figure 4-16 : Filtrate production in different 10 litres capacity clay ceramic filter dried at 850°C

4.8 CONCLUSION

A family of clay ceramics capable of submicron level water contaminant removal have been characterized and studied for its physical properties. The spectroscopic analysis showed the dominance of silica, alumina, and quartz, which contributed to building the strength of the fired ceramics. The presence of iron oxide was responsible for the reddish colour in the fired ceramics. The existence of the high amount of flux materials such as K_2O, Na_2O along with Fe_2O_3 have contributed in significant densification of porous ceramics (up to 50 percent organic fraction). The presence of Na_2O, K_2O, CaO, and MgO hints at the possible saline nature of the clay. Pores tend to be orthogonal irrespective of the volume fraction of raw materials which is representative of efficient filtration characteristics. Sample with 50 percent organic fraction was characterized by a large number of sub-micron pores and a large density of orthogonally orientated pores. The degree of the surface roughness increased in proportion with the pore fraction. The compressive strength displayed polynomially decreasing trend with the increasing surface roughness of clay-organic filler based ceramics. The fracture toughness of porous clay ceramics showed linear decrement with the increasing surface roughness. Fracture toughness was modelled based on raw material composition and it followed a linear transformation. The implications of the results will assist in the optimization of structural properties by studying the surface parameters of similar porous ceramics with application in the area of drinking water purification. Scaling of such filters is a viable way to increase filtrate production.

…